Check for updates

A new method for synthesizing ordered microporous carbons with tunable pore size and their application in pollutant removal†

Pan Ni, [ORCID] ab Xiaoqing He,cd Feng Xiao*ab and Baolin Deng*ab

Two ordered microporous carbons (0.83 nm and 1.55 nm) were synthesized for the first time via a modified silica template method, enabling the adjustment of the carbon microporous structure, which is a limitation of the conventional zeolite template method. Dye adsorption showed that its removal rate increased with decreasing pore size.

Since ordered microporous/mesoporous carbons (OMCs) were invented in 1997–2001;[1–4] their unique properties, including ordered open pore structure, high pore volume, high specific surface area, uniform pore size distributions, high conductivity, and high chemical stability, have attracted much attention from many researchers. New applications of these OMCs constantly emerge in the fields of water purification, enzyme immobilization, gas storage and separation, catalysis, supercapacitors, batteries, and fuel cells.[5,6]

Currently, the only reported method for synthesizing microporous OMCs is based on the Kyotani group's work using zeolites as templates such as zeolite Y, β, L, ZSM-5, and mordenite.[4,7–9] However, due to the wall thickness of less than 1 nm for zeolites, the pore size of the synthesized ordered carbon structure is limited to ≤1 nm because these reported microporous OMCs are the reverse replicas of their respective zeolite templates.[6,8] For potential applications in gas separation or water remediation where the target species may require a slightly larger micropore, for example, in the range of 1–2 nm,[6,10,11] the zeolite template method would not result in OMCs with a suitable porous structure.

aDepartment of Civil & Environmental Engineering, University of Missouri, Columbia, MO 65211, USA. E-mail: feng.xiao@missouri.edu; dengb@missouri.edu
bMissouri Water Center, University of Missouri, Columbia, MO 65211, USA
cElectron Microscopy Core Facility, University of Missouri, Columbia, MO 65211, USA
dDepartment of Mechanical & Aerospace Engineering, University of Missouri, Columbia, MO 65211, USA
† Electronic supplementary information (ESI) available: Characterization and dye removal data are available in the Excel spreadsheet. See DOI: https://doi.org/10.1039/d4va00414k

Environmental significance

Water pollution is one of the current emerging crises we human beings are facing. Adsorbents such as granular activated carbon (GAC) are often used to remove pollutants. However, the selectivity of these adsorbents toward pollutants such as dyes is not satisfactory, especially in the presence of abundant competing species. Elimelech et al. proposed subnanometer pores as the core to enhance the selectivity of single species.[53] However, achieving such pores in carbon adsorbents is extremely difficult. Our current work overcomes this barrier and makes it possible to study the pore size effect of five different OMCs with the same p6mm structure but varying pore sizes from 0.83 nm to 5.3 nm. Our dye sorption test confirmed the hypothesis that subnanometer pores can significantly enhance the selectivity of the target pollutant in the presence of competing species. The results of this work may shed light on next-generation GAC development.

In the pioneering studies using self-assembly of silica species and surfactants to synthesize mesoporous silica like MCM-41 and SBA-15, it was suggested that MCM-41 or SBA-15 with variable pore diameters could be synthesized by changing solution chemistry and the chain length of the utilized surfactants.[12–14] The feasibility of this feasibility was soon confirmed, and MCM-41 with a 2–10 nm pore size (ref. 13) and SBA-15 with a 5–30 nm pore size were successfully synthesized.[14] Based on these ordered mesoporous silica templates, the Ryoo and Jun group synthesized the world's first ordered mesoporous carbons (OMCs).[1–3] However, the pore size of the OMCs based on these ordered porous silica templates was never reported to be less than 2 nm. This is understandable because these silica templates had wall thicknesses ranging from 3.1 to 6.4 nm,[14] and the removal of the silica template would form ordered mesoporous OMCs with comparable pore sizes.

So far, quite a few studies have focused on the pore size adjustment of OMCs.[14–20] The key factors determining the pore size of these carbons include the carbon chain length of the surfactants (e.g., $EO_5PO_{70}EO_5$, $EO_{13}PO_{70}EO_{13}$, and $EO_{20}PO_{70}EO_{20}$),[14,15] the types of surfactants and their mixture ratios (e.g., P-123, F127, and CTAB),[15–17] the hydrothermal treatment

Table 1 Comparison of the current OMC synthesis methods and pore size adjustment conditions

Template synthesis				OMC synthesis					
Surfactant	Template precursor	T (°C)	Reaction time (h)[a]	Template	Carbon precursor	Reaction time	Pore size (nm)	Struct.	Ref.
$EO_5PO_{70}EO_5$ $EO_{13}PO_{70}EO_{13}$ $EO_{20}PO_{70}EO_{20}$ $EO_{20}PO_{70}EO_{20}$ $EO_{20}PO_{70}EO_{20}$ $EO_{20}PO_{70}EO_{20}$	TEOS	35 60 35 80 90 100	11–72	SBA-15	N/A	N/A	3.5[b] 3.4[b] 6.4[b] 5.3[b] 3.6[b] 3.1[b]	N/A	14 and 15
N/A	N/A	N/A	N/A	Y-zeolite SBA-15	Poly(acrylonitrile) for microporous OMCs	6 h at 100 °C	1.0	*Fd3m*	10 and 11
P-123 or $EO_{20}PO_{70}EO_{20}$	Sodium silicate	100	12	SBA-15	Sucrose	6 h at 160 °C 6 h at 900 °C under vacuum	3.8	*p6mm*	
HTAB : $C_{16}EO_8$ = 3 : 0 HTAB : $C_{16}EO_8$ = 2 : 1 HTAB : $C_{16}EO_8$ = 1 : 2 HTAB : $C_{16}EO_8$ = 0 : 3	Sodium silicate	100	12	SBA-15	Sucrose	6 h at 100 °C 6 h at 160 °C 6 h at 900 °C under vacuum	2.2 2.7 2.9 3.3	*p6mm* for all	16 and 17
Cetyltrimethylammonium bromide (CTAB)	TEOS	80	2	MCM-41	Sucrose	6 h at 100 °C 6 h at 160 °C NA at 900 °C under N_2	4.0	*p6mm*	19
P-123	Sodium silicate or TEOS	100	24	KIT-6	Sucrose furfuryl alcohol	6 h at 100 °C 6 h at 160 °C 6 h at 900 °C under vacuum	3.0 5.5	*Ia3d* for all	23 and 24
P-123 : F127 = 1 : 2.3	TEOS	100	12 24 72 168	SBA-16	Furfuryl alcohol Acenaphthene	1 h at 100 °C 2 h at 350 °C NA at 900 °C under vacuum	3.9 4.7 5.76 6.29	*Im3m* for all	18
$C_{16}H_{33}N(CH_3)_3Br$ $C_{12}H_{25}O(C_2H_4O)_4H$ or CTAB	TEOS	100	24	MCM-48	Sucrose	NA at 800–1100 °C under vacuum	3.0	*Ia3d*	1
P-123	TEOS	90	24	SBA-15	Sucrose	6 h at 100 °C 6 h at 160 °C 6 h at 700 °C 900 °C, 1100 °C under N_2	3.86 4.89 4.40	*p6mm* for all	25
P-123	TEOS	40 80 100 120 140	24	SBA-15	Sucrose	6 h at 100 °C 6 h at 160 °C 6 h at 890 °C under N_2	5.33 4.23 2.98 1.55 0.83	*p6mm* for all	This work

[a] The reaction time does not include the time of precursor dissolution, which is 20 h in this work. Additionally, the incineration time of the synthesized template to remove organic matter is not included to simplify the table. [b] The pore size is predicted from the silica wall thickness of the template since the structure of OMCs is the reverse replica of the silica template.

temperature (35–100 °C in general),[14] the hydrothermal treatment time (e.g., 12–168 h),[18] the types of templates and related modifications (e.g., SBA-15, SBA-16, zeolite, MCM-41, and MCM-48),[1,10,11,19–22] the carbon precursors (e.g., sucrose, furfuryl alcohol, acenaphthene, and acetonitrile),[18,23,24] carbonization methods (e.g., pyrolysis heating or chemical vapor deposition)[16,17,20–22] and pyrolysis temperature (e.g., 700–1100 °C).[25] The details are summarized in Table 1. Despite these efforts a method for adjusting pore size with a wide pore range of both micropores and mesopores while retaining the same carbon structure has not yet been reported.

Inspired by previous studies by others,[1–3,12–14] herein, we report a new approach via a revised silica template method to tune the porous structure of OMCs in a wide pore size range from 0.83 nm to 5.33 nm without changing the carbon structure, overlapping both microporous and mesoporous domains. This approach overcomes the shortcomings of the limited pore

size range of microporous OMCs obtained via the zeolite method (≤1 nm), making it possible to customize different micropore sizes of OMCs for any desired applications. As far as we know, other methods that enable pore size adjustment to cover both microporous and mesoporous carbon media have to compromise and change the carbon structure[10,26,27] (see Table 1).

These microporous and mesoporous OMCs were synthesized using SBA-15 with varying silica wall thicknesses as a template. Specifically, 8 grams of Pluronic P-123 (white gel, MW ~5800) was added into 300 mL of 2 M HCl solution and stirred for 10 h at 40 °C for its complete dissolution. Subsequently, 16.64 grams of tetraethyl orthosilicate (TEOS) was added into the solution and stirred for 20 hours at 40 °C. The resultant milky solution was placed in a 500 mL Teflon-sealed autoclave and heated in an oven at 80, 100, 120, and 140 °C for 24 h. For the synthesis of the largest mesopore OMC, the milky solution did not need to be transferred to the Teflon-sealed autoclave because the
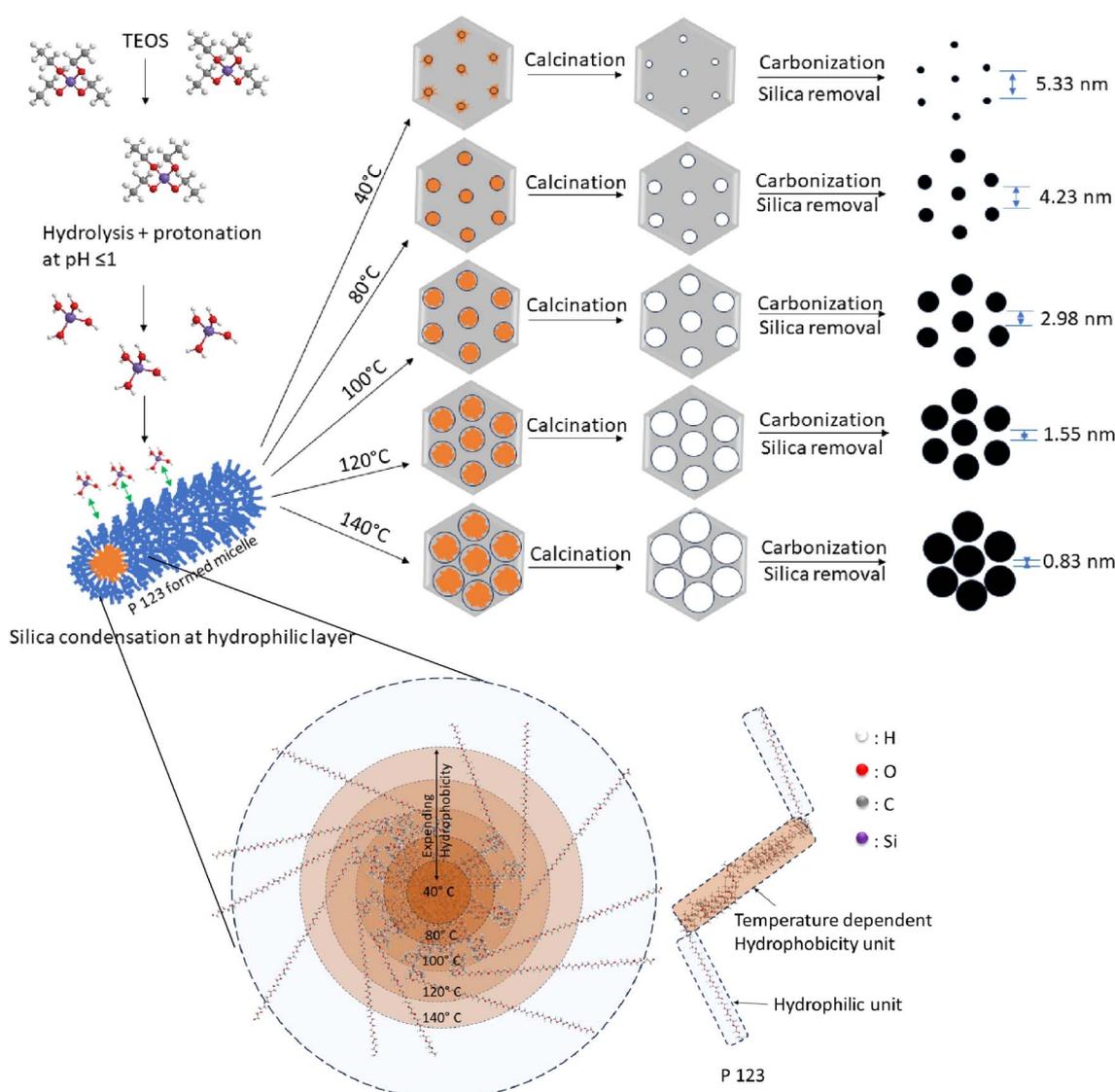

Fig. 1 A schematic illustration of the temperature-controlled method for synthesizing OMCs with micropore and mesopore sizes. The temperature error of the oven is ±1 °C.

© 2025 The Author(s). Published by the Royal Society of Chemistry

Environ. Sci.: Adv., 2025, 4, 1403–1411 | 1405

required heating temperature was relatively low, at 40 °C. We found that the key factor controlling the wall thickness of the silica template (or the pore size of the OMCs) was the temperature in this step. The mechanism was related to the temperature-dependent hydrophobicity of the poly(propylene glycol) units of the amphiphilic block copolymers (Pluronic P-123).[14] A higher temperature would enable the expansion of the hydrophobic unit (orange coloured area in Fig. 1), while compacting the hydrophilic unit (blue or light blue area in Fig. 1) of Pluronic P-123, leading to the larger pore size and thinner wall thickness of the silica templates. After cooling, the snow-white slurry was filtered without washing. The collected product was heated to 500 °C in air at a ramping rate of 1 °C min^{-1} and kept at this temperature for 6 h to remove the organic template P123. Based on the different temperatures applied in the hydrothermal treatment step, the obtained SBA-15 silica templates used for the synthesis of the two microporous OMCs were named SBA-15-120 and SBA-15-140, respectively, while the silica templates used for the synthesis of the three mesopore OMCs were named SBA-15-40, SBA-15-80, and SBA-15-100, respectively.

In the OMC synthesis step, except for the difference in the silica templates, all other protocols were the same. Specifically, 4.93 grams of SBA-15 was mixed with 24.7 mL of aqueous solution containing 6.16 grams of sucrose (≥99.5%) and 0.69 grams of H_2SO_4 (95.0–98.0%). The resulting white slurry was well stirred for 30 minutes and then placed in the oven for 6 h at 100 °C, followed by 160 °C for 6 h. The treated samples turned black. To obtain fully carbonized sucrose inside the pores of the silica template SBA-15, 3.94 grams of sucrose, 0.44 grams of H_2SO_4 and 24.7 mL deionized water were added to the samples again and the same heating cycle (100 °C for 6 h and 160 °C for 6 h) was applied as described above. The composite was pyrolyzed in a nitrogen flow (120 mL min^{-1}) inside an MTI GSL 1600X tube furnace with a ramping rate of 5 °C min^{-1} to 890 °C and treated at this temperature for 6 h to further carbonize the loaded carbon precursor within the silica templates. Thereafter, the obtained product was stirred in 100 mL of 4 M NaOH for 4 h to completely dissolve the silica template. Then, it was filtered and washed with deionized water until the pH of the rinsed water was in the range of 7.2–7.8. The collected OMCs were dried at 120 °C in the oven for 4 h and were then ground into powders, sealed, and stored in 20 mL glass vials before usage. The specific and unique synthesis conditions compared to other methods are summarized in Table 1.

High-resolution transmission electron microscopy (HRTEM) results (see Fig. 2a–e) confirmed the pore size of the five types of OMCs. They were 0.83 nm, 1.55 nm, 2.98 nm, 4.23 nm, and 5.33 nm, respectively. The details of the measurement of the pore size are shown in Fig. S1.† Briefly, 15 spots in each HRTEM photo were randomly chosen and measured using the scale bar in the original photo of each OMC and ImageJ software. The average pore size of 15 measurements was adopted. It should be noted that pore size determined by HRTEM is common in OMC and SBA-15 studies.[2,14] For convenience of discussion, these five OMCs were named after their pore size as OMC-0.83, OMC-1.55, OMC-2.98, OMC-4.23, and OMC-5.33.
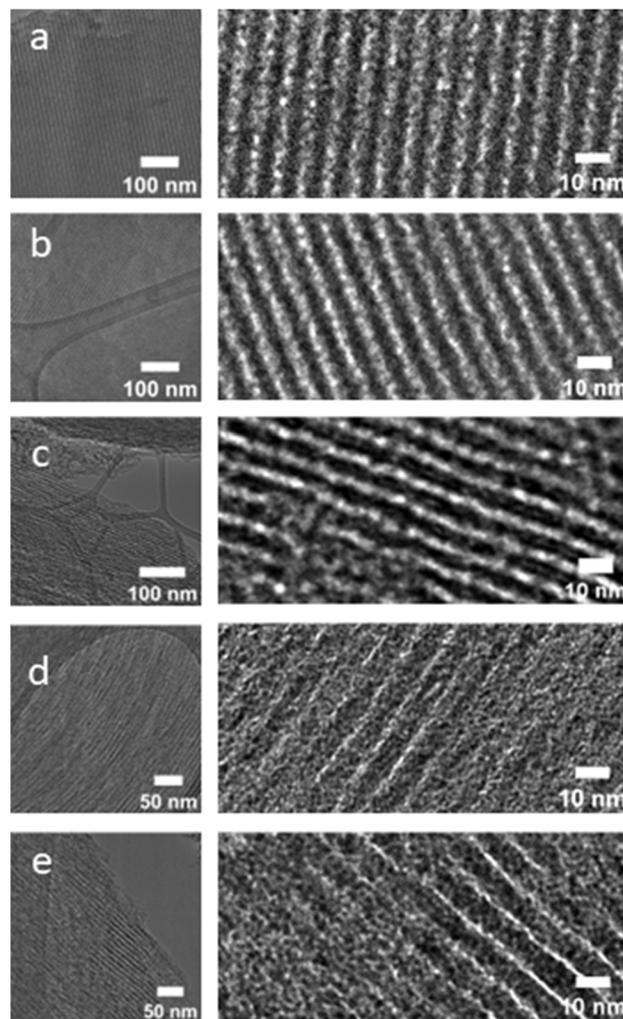

Fig. 2 High-resolution transmission electron microscopy (HRTEM) photos of OMCs with pore sizes of 5.33 (a), 4.23 (b), 2.98 (c), 1.55 (d), and 0.83 (e) nm, respectively.

The XRD analysis results of these five OMCs are shown in Fig. 3. The three peaks which represent (100), (110) and (200) diffractions of the hexagonal space group (*p6mm*) (ref. 2) were observed, suggesting that their carbon structures remain the same as the pore size varies. An interesting trend of these peaks becoming broader, weaker and shifting to the right as pore size decreases is consistent with other research groups' work on the synthesis of different mesopore OMCs.[16,17] This phenomenon is suggested to be caused by the smaller individual crystalline domains within the OMCs as the pore size of the media decreases.[28]

Additional N_2 sorption and desorption experiments and analysis through the Non-local Density Functional Theory (DFT) pore size distribution identified the dominant pores and average pore size, which are consistent with the HRTEM measured size. The slight difference may be caused by the diffusion limitation of nitrogen[29,30] (see Fig. S2† and Table 2). The surface area, total pore volume and micropore volume followed the same trend in the order: OMC-0.83 > OMC-1.55 > OMC-2.98 > OMC-4.23-OMC-5.33, with OMC-0.83 showing the
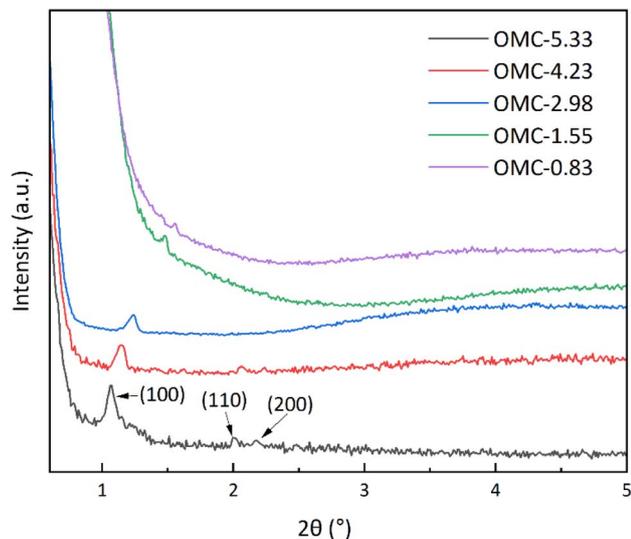
1406 | *Environ. Sci.: Adv.*, 2025, **4**, 1403–1411

© 2025 The Author(s). Published by the Royal Society of Chemistry

Fig. 3 XRD patterns of the five types of OMCs.

largest surface area of 402.7 m^2 g^{-1}, total pore volume of 0.43 cm^3 g^{-1}, and micropore volume of 0.15 cm^3 g^{-1} (see Fig. S3† and Table 2). Besides, for the 3 types of mesoporous OMCs in this case, micropores were also detected, as shown in Fig. S2† and Table 2. This phenomenon is consistent with other studies.[1,31,32] Accordingly, two possible reasons induce the formation of micropores: (1) preparation inhomogeneities in the carbon precursor filling, polymerization and carbonization processes. (2) the presence of micropores inside the carbon rods.[31] Raman spectra of all OMCs revealed a typical D band at 1329 cm^{-1} and a G band at 1595 cm^{-1} (see Fig. S4†). This is similar to the granular activated carbons (GAC), suggesting these OMCs were made of the defective, amorphous carbon and ordered graphitic crystallites of carbon.[10] The ratio of these band peaks (I_D/I_G) indicates the relative amount of defective carbon in the samples.[33] As is shown in Table S1,† the I_D/I_G of the five OMCs slightly increased as the pore size increased, suggesting that more defective carbon exists in the larger pore size OMCs. It is reported that defective carbon appears to be more important in pollutant removal.[34]

The hydrophobicity and surface charge of these OMCs were also characterized with the results shown in Fig. S5 and S6.† The contact angles of the five OMCs were comparable at around 130–147° with a slight decline as pore size increases, indicating strong hydrophobicity that is conducive to organic pollutant removal. The zeta potential analysis confirmed the negative charge of these OMCs at neutral pH and this negative surface charge was enhanced as the pore size increased.

To assess the removal of aqueous pollutants by these OMCs and explore the pore size effect on pollutant removal, two common dyes with opposite charges in the textile industry, methylene blue (MB, cationic dye)[35] and methyl orange (MO, anionic dye)[36] were selected in this case. Additionally, the effect of natural organic matter (NOM), a common component in surface water, was also investigated.

As is shown in Fig. 4, the loading capacity of both MB and MO among the five OMCs appeared to be pore-size dependent. OMC-0.83 obtained the highest q_e, 163.9 ± 0.5 mg g^{-1} for MB and 128.3 ± 4.4 mg g^{-1} for MO, respectively. The relatively lower removal of MO is likely to be caused by the electrostatic repulsion between the OMCs and the anionic dye molecules (see Fig. S6†). For MB, the adsorption capacity increased by 627.1% (based on average q_e), while for MO, the loading capacity was enhanced by 368.2% as the pore size lowered to 0.83 nm from 5.33 nm. This phenomenon could be caused by the increasing surface area of the OMCs with decreasing pore size (see Fig. S3† and Table 2). To clarify this, the loading capacity (q_e) in Fig. 4 was normalized with BET surface area data in Table 2 and the results are shown in Fig. 5. Interestingly, this pore-size dependent dye removal trend was still observed. Linear fitting suggests that there is a strong negative correlation between the pore size and the dye removal ability of OMCs and the surface area has little effect on it. Apart from the pore size effect, hydrophobicity may also play an important role. Accordingly, the higher hydrophobicity of GAC is likely to promote the removal of dyes.[37] The contact angle data in Fig. S5† showed a slight decrease as the pore size of the OMCs increases, indicating that the hydrophobicity difference in our case may also partly contribute to the results in Fig. 4 and 5. For the factor of surface charge of adsorbents, the reverse trend between cationic MB removal in Fig. 4 and zeta potential in Fig. S6† suggests that it contributes little to the pore-size dependent dye removal observed in this case. Similarly, defective carbons cannot be the dominant factor in dye removal as larger pore OMCs with more defective carbons removed smaller amounts of dyes. In addition, differences in the diffusion rates of MB and MO within these different pore channels may contribute to this pore size effect due to confinement in restricted space within the pores.[38]

Table 2 Surface area and pore size information of OMCs based on N$_2$ sorption and desorption

Carbon	BET surface area (m^2 g^{-1})	Total pore volume^a (cm^3 g^{-1})	Dom. pore size (nm)	Avg. pore size (nm)	Micro-volume^b (cm^3 g^{-1})
OMC-0.83	402.7	0.43	0.46, 0.59	0.57	0.15
OMC-1.55	397.9	0.44	0.54, 1.18	1.10	0.13
OMC-2.98	324.3	0.26	0.46, 4.32	3.97	0.13
OMC-4.23	247.9	0.19	0.59, 4.32	4.30	0.12
OMC-5.33	226	0.10	0.59, 5.43	5.42	0.06

^{a} Total pore volume was measured *via* the DFT model. ^{b} Micro-volume was measured *via* the DFT model. Dom. is dominant. Avg. is average and Micro is micropore.
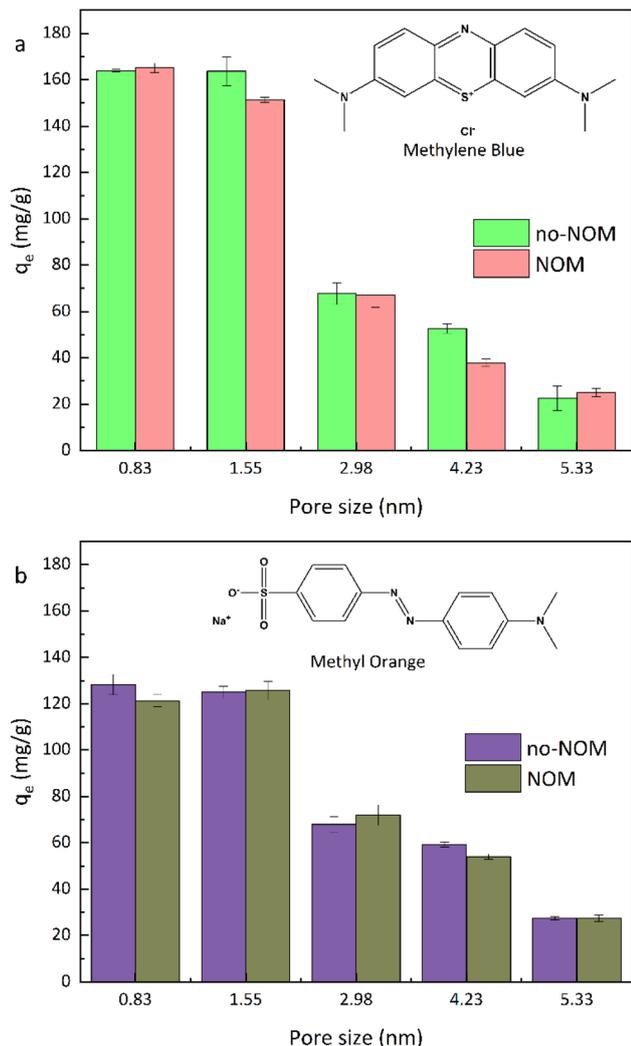
Fig. 4 Cationic dye (methylene blue, (a) and anionic dye (methyl orange, (b) adsorption capacity of OMCs at different pore sizes (NOM concentration is 10 mg L^{-1} humic acid). ChemDraw was used to draw the two dyes' structure.

Another possibility is the curvature of the pore channels within OMCs. The interaction forces such as electrostatic attraction and van der Waals between oppositely charged MB and OMCs may be enhanced due to the stronger curvature of the pores as pore size decreases.[26,27]

Interestingly, the addition of 10 mg L^{-1} NOM has almost no effect on both MB and MO removal by these OMCs. In addition to molecular weight differences likely existing between the dye and humic acid, humic acids were anionic species at neutral pH in water due to the presence of carboxylic and phenolic acid groups (used in our case to represent NOM), while MB carries a positive charge. The negative surface charge of OMCs would repulse the NOM while attracting cationic MB. That electrostatic repulsion between NOM and OMCs may contribute to the observed results in Fig. 4a.

For the removal of anionic dye MO, similar to MB, there was no significant inhibition by 10 mg L^{-1} humic acids observed, only a slight 5.5–8.6% in the OMC-0.83 and OMC-4.23 treated
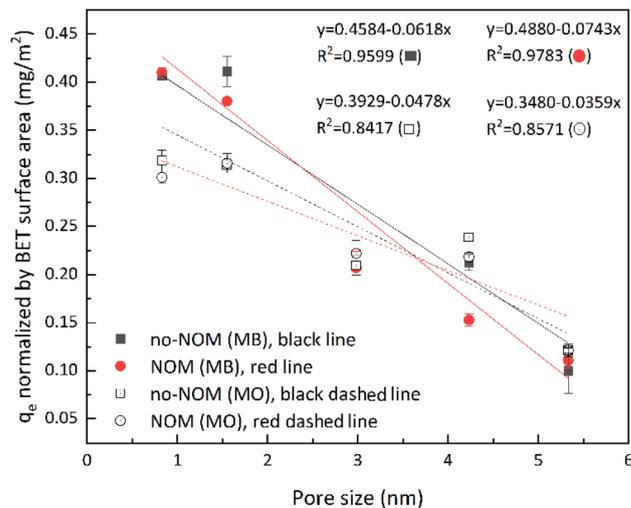

Fig. 5 BET surface area normalized adsorption capacity of OMCs for methylene blue and methyl orange at different pore sizes (NOM concentration is 10 mg L^{-1} humic acid).

groups. It is reported that the removal of pollutants like 2-methylisoborneol and per- and polyfluoroalkyl substances (PFAS) can be significantly inhibited by NOM.[39,40] One possible reason for our results is related to the molecular size of the humic acid. The size of humic acids can vary from 500 Da to over 100 000 Da.[41] The size of our humic acid (53680-10 G, technical grade, Sigma Aldrich) is estimated to be 20 000–50,000 Da. Newcombe *et al.* reported that only humic acid molecules smaller than 3000 Da can cause significant competition inhibition, and for larger humic acid molecules, due to the size exclusion effect, there may not be any inhibition.[40] Another suggested reason is the high dose of OMCs used in our case. Yilmaz *et al.* reported that the inhibition effect by NOM is only significant when the activated carbon dose is low at 10–75 mg L^{-1}.[42] Our dose is much higher at 1 g L^{-1}.

More data on the MB and MO removal rates and the colour change in dye solutions are shown in Fig. S7–S10.† For 200 mg L^{-1} MB or MO solution, OMC-0.83 removed 82.2 ± 0.3% of MB and 63.1 ± 2.2% of MO, while that of OMC-5.33 was only 11.3 ± 2.7% of MB and 13.5 ± 0.4% of MO. The performance difference of these two dyes, as discussed before, is likely due to the electrostatic repulsion between anionic MO and negatively charged surfaces of OMCs. There are many studies focusing on MB and MO removal by activated carbon and other adsorbents.[43–52] The performance comparison between this work and previous studies is summarized in Table S2.† It is shown that the MB and MO loading capacity of our OMC-0.83 is comparable to the reported best ones, indicating that it is an efficient adsorbent for dye removal and our strategy to lower the pore size of carbon adsorbents to enhance dye removal is feasible.

It should be noted that the studies of the pore size effect on dye or other target species removal using carbon materials such as OMCs and carbon nanotubes or CNTs have been conducted previously by others.[10,26,27] In those studies, however, the carbon structures of either OMCs (*e.g.*, Y-zeolite templates for

microporous OMCs and SBA-15 for mesopore OMCs) or CNTs (e.g., single wall CNTs and multi-wall CNTs) have completely changed when attempting to adjust the pore size. This makes it very difficult to clarify the effect of structural changes and pore size changes separately. In contrast, in this study, the effect of structural changes is excluded as the five OMCs have the same hexagonal structure (see Fig. 3). As far as we know, this study is the first to evaluate dye adsorption using microporous and mesoporous OMCs without changing the OMC structure.

In summary, a new way to synthesize microporous OMCs with tunable pore size was introduced. It overcomes the limitations of the zeolite template method that only allows the synthesis of OMCs with pore size ≤1 nm and makes it possible to synthesize microporous OMCs with a broader range of pore sizes spanning from microporous to mesoporous domains. Besides, we found that both cationic MB and anionic MO removal by these OMCs was pore-size dependent. The smaller the pore size, the better the removal performance toward the dyes from water. This new synthesis method may boost the applications of OMCs in molecule sieves, gas separation/storage, batteries, water remediation, and many other fields.

Data availability

Data are available in the shared Excel file and ESI file.†

Conflicts of interest

There are no conflicts to declare.

Acknowledgements

Notes and references

1 R. Ryoo, S. H. Joo and S. Jun, Synthesis of highly ordered carbon molecular sieves via template-mediated structural transformation, J. Phys. Chem. B, 1999, 103, 7743–7746.

2 S. Jun, S. H. Joo, R. Ryoo, M. Kruk, M. Jaroniec, Z. Liu, T. Ohsuna and O. Terasaki, Synthesis of new, nanoporous carbon with hexagonally ordered mesostructure, J. Am. Chem. Soc., 2000, 122, 10712–10713.

3 R. Ryoo, S. H. Joo, M. Kruk and M. Jaroniec, Ordered mesoporous carbons, Adv. Mater., 2001, 13, 677–681.

4 T. Kyotani, T. Nagai, S. Inoue and A. Tomita, Formation of new type of porous carbon by carbonization in zeolite nanochannels, Chem. Mater., 1997, 9, 609–615.

5 M. E. Davis, Ordered porous materials for emerging applications, Nature, 2002, 417, 813–821.

6 J. Lee, J. Kim and T. Hyeon, Recent progress in the synthesis of porous carbon materials, Adv. Mater., 2006, 18, 2073–2094.

7 Z. X. Ma, T. Kyotani, Z. Liu, O. Terasaki and A. Tomita, Very high surface area microporous carbon with a three-dimensional nano-array structure: Synthesis and its molecular structure, Chem. Mater., 2001, 13, 4413–4415.

8 T. Kyotani, Z. X. Ma and A. Tomita, Template synthesis of novel porous carbons using various types of zeolites, Carbon, 2003, 41, 1451–1459.

9 Z. X. Ma, T. Kyotani and A. Tomita, Preparation of a high surface area microporous carbon having the structural regularity of Y zeolite, Chem. Commun., 2000, 2365–2366.

10 L. L. Ji, F. L. Liu, Z. Y. Xu, S. R. Zheng and D. Q. Zhu, Adsorption of Pharmaceutical Antibiotics on Template-Synthesized Ordered Micro- and Mesoporous Carbons, Environ. Sci. Technol., 2010, 44, 3116–3122.

11 L. L. Ji, F. L. Liu, Z. Y. Xu, S. R. Zheng and D. Q. Zhu, Zeolite-Templated Microporous Carbon As a Superior Adsorbent for Removal of Monoaromatic Compounds from Aqueous Solution, Environ. Sci. Technol., 2009, 43, 7870–7876.

12 C. T. Kresge, M. E. Leonowicz, W. J. Roth, J. C. Vartuli and J. S. Beck, Ordered Mesoporous Molecular-Sieves Synthesized by a Liquid-Crystal Template Mechanism, Nature, 1992, 359, 710–712.

13 J. S. Beck, J. C. Vartuli, W. J. Roth, M. E. Leonowicz, C. T. Kresge, K. D. Schmitt, C. T. W. Chu, D. H. Olson, E. W. Sheppard, S. B. McCullen, J. B. Higgins and J. L. Schlenker, A New Family of Mesoporous Molecular-Sieves Prepared with Liquid-Crystal Templates, J. Am. Chem. Soc., 1992, 114, 10834–10843.

14 D. Y. Zhao, J. L. Feng, Q. S. Huo, N. Melosh, G. H. Fredrickson, B. F. Chmelka and G. D. Stucky, Triblock copolymer syntheses of mesoporous silica with periodic 50 to 300 angstrom pores, Science, 1998, 279, 548–552.

15 D. Y. Zhao, Q. S. Huo, J. L. Feng, B. F. Chmelka and G. D. Stucky, Nonionic triblock and star diblock copolymer and oligomeric surfactant syntheses of highly ordered, hydrothermally stable, mesoporous silica structures, J. Am. Chem. Soc., 1998, 120, 6024–6036.

16 J. S. Lee, S. H. Joo and R. Ryoo, Synthesis of mesoporous silicas of controlled pore wall thickness and their replication to ordered nanoporous carbons with various pore diameters, J. Am. Chem. Soc., 2002, 124, 1156–1157.

17 R. Ryoo and S. H. Joo, Nanostructured carbon materials synthesized from mesoporous silica crystals by replication, Stud. Surf. Sci. Catal., 2004, 148, 241–260.

© 2025 The Author(s). Published by the Royal Society of Chemistry

Environ. Sci.: Adv., 2025, 4, 1403–1411 | 1409

18 T. W. Kim, R. Ryoo, K. P. Gierszal, M. Jaroniec, L. A. Solovyov, Y. Sakamoto and O. Terasaki, Characterization of mesoporous carbons synthesized with SBA-16 silica template, J. Mater. Chem., 2005, 15, 1560–1571.

19 C. F. Lin, X. Zhang, H. Lin, N. Wang, J. B. Li and X. Z. Yang, Synthesis of ordered mesoporous carbon using MCM-41 mesoporous silica as template, Adv. Mater. Res., 2006, 11–12, 543–546.

20 S. B. Singh and M. De, Alumina based doped templated carbons: A comparative study with zeolite and silica gel templates, Microporous Mesoporous Mater., 2018, 257, 241–252.

21 S. B. Singh and M. De, Scope of doped mesoporous (<10 nm) surfactant-modified alumina templated carbons for hydrogen storage applications, Int. J. Energy Res., 2019, 43, 4264–4280.

22 S. B. Singh, P. Hajare, R. J. Konwar and M. H. Y. De, Physically and chemically modified zeolite templated nitrogenous carbons for enhanced hydrogen adsorption, Flatchem, 2024, 48, 100767.

23 Y. Seo, K. Kim, Y. Jung and R. Ryoo, Synthesis of mesoporous carbons using silica templates impregnated with mineral acids, Microporous Mesoporous Mater., 2015, 207, 156–162.

24 F. Kleitz, S. H. Choi and R. Ryoo, Cubic Ia3d large mesoporous silica: synthesis and replication to platinum nanowires, carbon nanorods and carbon nanotubes, Chem. Commun., 2003, 2136–2137.

25 X. B. Lei, L. U. Yao, Q. Y. Lian, X. Zhang, T. J. Wang, W. Holmes, G. Y. Ding, D. D. Gang and M. E. Zappi, Enhanced adsorption of perfluorooctanoate (PFOA) onto low oxygen content ordered mesoporous carbon (OMC): Adsorption behaviors and mechanisms, J. Hazard. Mater., 2022, 421.

26 X. Chen, X. H. Xia, X. L. Wang, J. P. Qiao and H. T. Chen, A comparative study on sorption of perfluorooctane sulfonate (PFOS) by chars, ash and carbon nanotubes, Chemosphere, 2011, 83, 1313–1319.

27 S. B. Deng, Q. Y. Zhang, Y. Nie, H. R. Wei, B. Wang, J. Huang, G. Yu and B. S. Xing, Sorption mechanisms of perfluorinated compounds on carbon nanotubes, Environ. Pollut., 2012, 168, 138–144.

28 T. Ungar, Microstructural parameters from X-ray diffraction peak broadening, Scr. Mater., 2004, 51, 777–781.

29 Z. Y. Wang, A. Alinezhad, S. Nason, F. Xiao and J. J. Pignatello, Enhancement of per- and polyfluoroalkyl substances removal from water by pyrogenic carbons: Tailoring carbon surface chemistry and pore properties, Water Res., 2023, 229, 119467.

30 S. Dantas, K. C. Struckhoff, M. Thommes and A. V. Neimark, Pore size characterization of micro-mesoporous carbons using CO$_2$ adsorption, Carbon, 2021, 173, 842–848.

31 T. Onfroy, F. Guenneau, M. A. Springuel-Huet and A. Gédéon, First evidence of interconnected micro and mesopores in CMK-3 materials, Carbon, 2009, 47, 2352–2357.

32 J. Dobrzynska, K. Morlo, R. Olchowski and R. Dobrowolski, Modified CMK-3 carbon materials for efficient removal of roxarsone, Appl. Surf. Sci., 2024, 674, 160934.

33 A. C. Ferrari and J. Robertson, Interpretation of Raman spectra of disordered and amorphous carbon, Phys. Rev. B, 2000, 61, 14095–14107.

34 L. He, Y. Y. Qiu, C. Yao, G. J. Lan, N. Li, H. C. Zhou, Q. S. Liu, X. C. Sun, Z. Z. Cheng and Y. Li, Role of intrinsic defects on carbon adsorbent for enhanced removal of Hg2+ in aqueous solution, Chin. J. Chem. Eng., 2023, 61, 129–139.

35 L. Mouni, L. Belkhiri, J. C. Bollinger, A. Bouzaza, A. Assadi, A. Tirri, F. Dahmoune, K. Madani and H. Remini, Removal of Methylene Blue from aqueous solutions by adsorption on Kaolin: Kinetic and equilibrium studies, Appl. Clay Sci., 2018, 153, 38–45.

36 L. J. Wu, X. W. Liu, G. C. Lv, R. L. Zhu, L. T. Tian, M. Liu, Y. X. Li, W. X. Rao, T. M. Liu and L. B. Liao, Study on the adsorption properties of methyl orange by natural one-dimensional nano-mineral materials with different structures, Sci. Rep., 2021, 11, 10640.

37 E. I. El-Shafey, S. N. F. Ali, S. Al-Busafi and H. A. J. Al-Lawati, Preparation and characterization of surface functionalized activated carbons from date palm leaflets and application for methylene blue removal, J. Environ. Chem. Eng., 2016, 4, 2713–2724.

38 W. Wang, Y. Jia, S. X. Zhou and S. B. Deng, Removal of typical PFAS from water by covalent organic frameworks with different pore sizes, J. Hazard. Mater., 2023, 460.

39 J. Yu, L. Lv, P. Lan, S. J. Zhang, B. C. Pan and W. M. Zhang, Effect of effluent organic matter on the adsorption of perfluorinated compounds onto activated carbon, J. Hazard. Mater., 2012, 225, 99–106.

40 G. Newcombe, M. Drikas and R. Hayes, Influence of characterised natural organic material on activated carbon adsorption: II. Effect on pore volume distribution and adsorption of 2-methylisoborneol, Water Res., 1997, 31, 1065–1073.

41 M. Zolfaghari, O. Dia, N. Klai, P. Drogui, S. K. Brar, G. Buelna and R. Dubé, Removal of Pollutants in Different Landfill Leachate Treatment Processes on the Basis of Organic Matter Fractionation, J. Environ. Qual., 2018, 47, 297–305.

42 E. Yilmaz, E. Altiparmak, F. Dadaser-Celik and N. Ates, Impact of Natural Organic Matter Competition on the Adsorptive Removal of Acetochlor and Metolachlor from Low-Specific UV Absorbance Surface Waters, ACS Omega, 2023, 8, 31758–31771.

43 H. M. Alghamdi, A. M. Elgarahy, M. S. Zoromba and K. Z. Elwakeel, A microwave-regenerable multi-walled carbon nanotube/polyaniline/Fe3O4 ternary nanocomposite for quantifiable sorption of cationic and anionic dyes, Colloids Surf., A, 2024, 698.

44 K. Z. Elwakeel, S. El-Kousy, H. G. El-Shorbagy and M. A. Abd El-Ghaffar, Comparison between the removal of Reactive Black 5 from aqueous solutions by 3-amino-1,2,4 triazole, 5-thiol and melamine grafted chitosan prepared through four different routes, J. Environ. Chem. Eng., 2016, 4, 733–745.

45 K. Z. Elwakeel, A. A. El-Bindary, A. Ismail and A. M. Morshidy, Sorptive removal of Remazol Brilliant Blue R from aqueous solution by diethylenetriamine functionalized magnetic macro-reticular hybrid material, *RSC Adv.*, 2016, **6**, 22395–22410.

46 K. Z. Elwakeel, M. A. Abd El-Ghaffar, S. M. El-kousy and H. G. El-Shorbagy, Synthesis of new ammonium chitosan derivatives and their application for dye removal from aqueous media, *Chem. Eng. J.*, 2012, **203**, 458–468.

47 K. Z. Elwakeel, Removal of Reactive Black 5 from aqueous solutions using magnetic chitosan resins, *J. Hazard. Mater.*, 2009, **167**, 383–392.

48 G. H. Al-Hazmi, A. Akhdhar, A. Shahat and K. Z. Elwakeel, Adsorption of Gentian violet dye onto mesoporous aluminosilica monoliths: nanoarchitectonics and application to industrial wastewater, *Int. J. Environ. Anal. Chem.*, 2024, **104**, 4415–4436.

49 K. Z. Elwakeel, A. Shahat, Z. A. Khan, W. Alshitari and E. Guibal, Magnetic metal oxide-organic framework material for ultrasonic-assisted sorption of titan yellow and rose bengal from aqueous solutions, *Chem. Eng. J.*, 2020, **392**, 123635.

50 Buhani, J. S. Dewi, N. S. Fajriyah, M. Rilyanti, Suharso, Sumadi and K. Z. Elwakeel, Modification of Non-Activated Carbon from Rubber Fruit Shells with 3-(Aminopropyl)-Triethoxysilane and Its Adsorption Study on Coomassie Brilliant Blue and Methylene Blue in Solution, *Water, Air, Soil Pollut.*, 2023, **234**, 578.

51 Buhani, Suharso, M. Rilyanti, F. D. R. Antika, L. P. Lestari, Sumadi, M. Ansori and K. Z. Elwakeel, Functionalization of carbon from rubber fruit shells (Hevea brasiliensis) with silane agents and its application to the adsorption of bi-component mixtures of methylene blue and crystal violet, *Environ. Sci. Pollut. Res.*, 2023, 39994–40007.

52 A. M. Elgarahy, H. Y. Mostafa, E. G. Zaki, S. M. ElSaeed, K. Z. Elwakeel, A. Akhdhar and E. Guibal, Methylene blue removal from aqueous solutions using a biochar/gellan gum hydrogel composite: Effect of agitation mode on sorption kinetics, *Int. J. Biol. Macromol.*, 2023, 232.

53 R. Epsztein, R. M. DuChanois, C. L. Ritt, A. Noy and M. Elimelech, *Nature Nanotechnology*, 2020, **15**, 426–436.

© 2025 The Author(s). Published by the Royal Society of Chemistry

Environ. Sci.: Adv., 2025, **4**, 1403–1411 | 1411